Quantum information diode based on a magnonic crystal

IOP Publishing Mater. Quantum Technol. 3 (2023) 035003 https://doi.org/10.1088/2633-4356/ace603

Materials for Quantum Technology

OPEN ACCESS

RECEIVED
28 February 2023

REVISED
13 June 2023

ACCEPTED FOR PUBLICATION
10 July 2023

PUBLISHED
1 August 2023

PAPER

Quantum information diode based on a magnonic crystal

Rohit K Shukla[1], Levan Chotorlishvili[2,*], Vipin Vijayan[1], Harshit Verma[3], Arthur Ernst[4,5,*], Stuart S P Parkin[4] and Sunil K Mishra[1,*]

[1] Department of Physics, Indian Institute of Technology (Banaras Hindu University), Varanasi 221005, India
[2] Department of Physics and Medical Engineering, Rzeszow University of Technology, 35-959 Rzeszow, Poland
[3] Centre for Engineered Quantum Systems (EQUS), School of Mathematics and Physics, The University of Queensland, St Lucia QLD 4072, Australia
[4] Max Planck Institute of Microstructure Physics, Weinberg 2, D-06120 Halle, Germany
[5] Institute of Theoretical Physics, Johannes Kepler University Alterger Strasse 69, 4040 Linz, Austria
* Authors to whom any correspondence should be addressed.

E-mail: levan.chotorlishvili@gmail.com, Arthur.Ernst@jku.at and sunilkm.app@iitbhu.ac.in

Keywords: magnonics, magnetism, quantum information

Abstract

Exploiting the effect of nonreciprocal magnons in a system with no inversion symmetry, we propose a concept of a quantum information diode (QID), i.e. a device rectifying the amount of quantum information transmitted in the opposite directions. We control the asymmetric left and right quantum information currents through an applied external electric field and quantify it through the left and right out-of-time-ordered correlation. To enhance the efficiency of the QID, we utilize a magnonic crystal. We excite magnons of different frequencies and let them propagate in opposite directions. Nonreciprocal magnons propagating in opposite directions have different dispersion relations. Magnons propagating in one direction match resonant conditions and scatter on gate magnons. Therefore, magnon flux in one direction is damped in the magnonic crystal leading to an asymmetric transport of quantum information in the QID. A QID can be fabricated from an yttrium iron garnet film. This is an experimentally feasible concept and implies certain conditions: low temperature and small deviation from the equilibrium to exclude effects of phonons and magnon interactions. We show that rectification of the flaw of quantum information can be controlled efficiently by an external electric field and magnetoelectric effects.

1. Introduction

A diode is a device designated to support asymmetric transport. Nowadays, household electric appliances or advanced experimental scientific equipment are all inconceivable without extensive use of diodes. Diodes with a perfect rectification effect permit electrical current to flow in one direction only. The progress in nanotechnology and material science passes new demands to a new generation of diodes; futuristic nano-devices that can rectify either acoustic (sound waves), thermal phononic, or magnonic spin current transport. Nevertheless, we note that at the nano-scale, the rectification effect is never perfect, i.e. backflow is permitted, but amplitudes of the front and backflows are different [1–14]. In the present work, we propose an entirely new type of diode designed to rectify the quantum information current. We do believe that in the foreseeable future the quantum information diode (QID) has a perspective to become a benchmark of quantum information technologies.

The functionality of a QID relies on the use of magnonic crystals, i.e., artificial media with a characteristic periodic lateral variation of magnetic properties. Similar to photonic crystals, magnonic crystals possess a band gap in the magnonic excitation spectrum. Therefore, spin waves with frequencies matching the band gap are not allowed to propagate through the magnonic crystals [15–21]. This effect has been utilized earlier to demonstrate a magnonic transistor in a yttrium iron garnet (YIG) strip [15, 16]. The essence of a magnonic transistor is a YIG strip with a periodic modulation of its thickness (magnonic crystal). The transistor is complemented by a source, a drain, and gate antennas. A gate antenna injects

magnonic crystal magnons with a frequency ω_G matching the magnonic crystal band gap. In the process, the gate magnons cannot leave the crystal and may reach a high density. Magnons emitted from a source with a wave vector $\mathbf{k}_s$ flowing towards the drain run into the magnonic crystal. The interaction between the source magnons and the magnonic crystal magnons is a four-magnon scattering process. The magnonic current emitted from the source attenuates in the magnonic crystal, and the weak signal reaches the drain due to the scattering. The relaxation process is swift if the following condition holds [16, 22]

$$k_s = \frac{m_0 \pi}{a_0}, \tag{1}$$

where m_0 is the integer, and a_0 is the crystal lattice constant. The magnons with wave vectors satisfying the Bragg conditions equation (1) will be resonantly scattered back, resulting in the generation of rejection bands in a spin-wave spectrum over which magnon propagation is entirely prohibited. Experimental verification of this effect is given in [16].

2. Results

2.1. Proposed set-up for QID

A pictorial representation of a QID is shown in figure 1. A magnonic crystal can be fabricated from an YIG film. Grooves can be deposited using a lithography procedure in a few nanometer steps, and, for our purpose, we consider parallel lines in width of 1 μm spaced with 10 μm from each other. Therefore, the lattice constant, approximately $a_0 = 11$ μm, *i.e.*, is much larger than the unit cell size $a = 10$ nm used in our coarse-graining approach. Due to the capacity of our analytical calculations, we consider quantum spin chains of length about $N = 1000$ spins and the maximal distance between the spins $r_{ij} = d$ (in the units of a), $d = i - j = 40$. In what follows, we take $k(\omega)a \ll 1$. The mechanism of the QID is based on the effect of direction dependence of nonreciprocal magnons [23–25]. In the chiral spin systems, the absence of inversion symmetry causes a difference in dispersion relations of the left and right propagating magnons, *i.e.* $\omega_{s,L}(\mathbf{k}) \neq \omega_{s,R}(-\mathbf{k})$. Due to the Dzyaloshinskii–Moriya interaction (DMI), magnons of the same frequency ω_s propagating in opposite directions have different wave vectors [26]: $a\,(k_s^+ - k_s^-) = D/J$, where J is the exchange constant, and D is the DMI constant. Therefore, if the condition equation (1) holds for the left propagating magnons, it is violated for the right propagating magnons and vice versa. These magnons propagating in different directions decay differently in the magnonic crystal. Without loss of generality, we assume that the right propagating magnons with k_s^+ satisfy the condition equation (1), and the current attenuates due to the scattering of source magnons by the gate magnons. The left propagating magnons k_s^- violate the condition equation (1), and the current flows without scattering. Thus, reversing the source and drain antennas' positions rectifies the current. Following [16], we introduce a suppression rate of the source to drain the magnonic current $\xi(D) = 1 - n_D^+/n_D^-$, where $n_D^+ < n_D^-$ are densities of the drain magnons with and without scattering. The parameter $\xi(D)$ is experimentally accessible, and it depends on a particular setup. Therefore, in this manuscript, we take $\xi(D)$ as a free theory parameter. Multiferroic (MF) materials are considered as a good example of a system with broken inversion symmetry, (see [27–35]) and references therein. MF properties of YIG are studied in [36]. Moreover, in accordance with scanning tunneling microscopy experiments, a change of the spin direction at one edge of a chiral chain was experimentally probed by tens of nanometers away from the second edge [35].

2.2. Model

We consider a 2D square-lattice spin system with nearest-neighbor J_1 and the next nearest-neighbor J_2 coupling constants:

$$\hat{H} = J_1 \sum_{\langle n,m \rangle} \hat{\sigma}_n \hat{\sigma}_m + J_2 \sum_{\langle\langle n,m \rangle\rangle} \hat{\sigma}_n \hat{\sigma}_m - \mathbf{P} \cdot \mathbf{E}, \tag{2}$$

where $\langle n,m \rangle$ and $\langle\langle n,m \rangle\rangle$ indicates all the pairs with nearest-neighbor and next nearest-neighbor interactions, respectively. The last term in equation (2) describes a coupling of the ferroelectric polarization with unit vector $\mathbf{e}^x_{i,i+1}$, $\mathbf{P} = g_{\rm ME}\mathbf{e}^x_{i,i+1} \times (\hat{\sigma}_i \times \hat{\sigma}_{i+1})$ with an applied external electric field and mimics an effective DMI term $D = E_y g_{\rm ME}$ breaking the left-right symmetry, where

$$-\mathbf{P} \cdot \mathbf{E} = D \sum_n (\hat{\sigma}_n \times \hat{\sigma}_{n+1})_z. \tag{3}$$

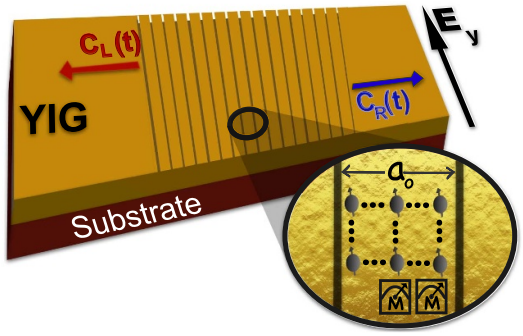

Figure 1. Illustration of a quantum information diode: a plane of a YIG film with grooves orthogonal to the direction of the propagation of quantum information. In the middle of the QID, we pump extra magnons to excite the system. A quantum excitation propagates toward the left, and the right ends asymmetrically. To describe the propagation process of quantum information, we introduce the left and right OTOC $C_L(t)$ and $C_R(t)$. Because the left-right inversion is equivalent to $D \to -D$ meaning $E_y \to -E_y$, we can invert the left and right OTOCs by switching the applied external electric field.

Here we consider only the nearest neighbor DMI and only in one direction. As a consequence, the left-right inversion is equivalent to $D \to -D$, or $E_y \to -E_y$. The broken left-right inversion symmetry can be exploited in rectifying the information current by an electric field. More importantly, the procedure is experimentally feasible. We can diagonalize the Hamiltonian in equation (2) by using the Holstein–Primakoff transformation [37–40] (see appendix A for detailed derivation) as:

$$\hat{H} = \sum_{\vec{k}} \omega(\pm D, \mathbf{k}) \hat{a}^{\dagger}_{\vec{k}} \hat{a}_{\vec{k}},\ \omega(\pm D, \mathbf{k}) = \left(\omega(\vec{k}) \pm \omega_{\mathrm{DM}}(\vec{k})\right),\ \ \omega_{\mathrm{DM}}(\vec{k}) = D \sin(k_x a),$$
$$\omega(\vec{k}) = 2J_1(1 - \gamma_{1,\mathbf{k}}) + 2J_2(1 - \gamma_{2,\mathbf{k}}),\ \gamma_{1,\mathbf{k}} = \frac{1}{2}(\cos k_x a + \cos k_y a),$$
$$\gamma_{2,\mathbf{k}} = \frac{1}{2}[\cos(k_x + k_y)a + \cos(k_x - k_y)a]. \tag{4}$$

Here $\pm D$ corresponds to the magnons propagating in opposite directions and the sign change is equivalent to the electric field direction change. We note that a 1D character of the DM term is ensured by the magnetoelectric effect [27] and to the electric field applied along the **y** axis.

The speed limit of information propagation is usually given in terms of Lieb–Robinson (LR) bound, defined for the Hamiltonians that are locally bounded and short-range interacting [41–43]. Since the Hamiltonian in equation (2) satisfies both conditions, the LR bound can be defined for the spin model. However, when we transform the Hamiltonian using Holstein–Primakoff bosons, we have to take extra care as the bosons are not locally bounded. To define LR bound, we take only a few noninteracting magnons and exclude the magnon–magnon interaction to truncate terms beyond quadratic operators. In a realistic experimental setting, low density of propagating magnons in YIG can easily be achieved by properly controlling the microwave antenna. In the case of low magnon density, the role of the magnon–magnon interaction between propagating magnons in YIG is negligible. Therefore, for YIG, we have a quadratic Hamiltonian, which is a precise approach in a low magnon density limit. Our discussion is valid for the experimental physical system [16], where magnons of YIG do not interact with each other, implying that there is no term in the Hamiltonian beyond quadratic. We can estimate LR bounds [44] defining the maximum group velocities of the left-right propagating magnons $v_g^{\pm}(\vec{k}) = \frac{\partial(\omega(\vec{k}) \pm \omega_{\mathrm{DM}}(\vec{k}))}{\partial k}$. Taking into account the explicit form of the dispersion relations, we see that the maximal asymmetry is approximately equal to the DM constant *i.e.* $v_g^{+}(0) - v_g^{-}(0) \approx 2\mathrm{D}$. We note that the effect of nonreciprocal magnons is already observed experimentally [45–49] but up to date, never discussed in the context of the quantum information theory.

We formulate the central interest question as follows: at $t = 0$, we act upon the spin $\hat{\sigma}_n$ to see how swiftly changes in the spin direction can be probed tens of sites away $d = n - m \gg 1$, and whether the forward and backward processes (i.e. probing for $\hat{\sigma}_m$ the outcome of the measurement done on $\hat{\sigma}_n$) are asymmetric or not. Due to the left-right asymmetry, the chiral spin channel may sustain a diode rectification effect when transferring the quantum information from left to right and in the opposite direction. We note that our discussion about the left-right asymmetry of the quantum information flow is valid until the current reaches boundaries. Thus the upper limit of the time reads $t_{\max} = Na/v_g^{\pm}(\vec{k})$, where N is the size of the system.

2.3. Out-of-time-order correlator (OTOC)

Larkin and Ovchinnikov [50] introduced the concept of the OTOC, and since then, OTOC has been seen as a diagnostic tool of quantum chaos. The concern of delocalizations in the quantum information theory (i.e. the scrambling of quantum entanglement) was renewed only recently, see [51–60] and references therein. OTOC is also used for describing the static and dynamical phase transitions [61–63]. Dynamics of the semi-classical, quantum, and spin systems can be discussed by using OTOC [51, 64–67]. We utilize OTOC to characterize the left-right asymmetry of the quantum information flow and thus infer the rectification effect of a diode.

Let us consider two unitary operators $\hat{V}$ and $\hat{W}$ describing local perturbations to the chiral spin system equation (2), and the unitary time evolution of one of the operators $\hat{W}(t) = \exp(i\hat{H}t)\hat{W}(0)\exp(-i\hat{H}t)$. Then the OTOC is defined as

$$C(t) = \frac{1}{2}\left\langle \left[\hat{W}(t), \hat{V}(0)\right]^{\dagger}\left[\hat{W}(t), \hat{V}(0)\right]\right\rangle, \tag{5}$$

where parentheses $\langle\cdots\rangle$ denotes a quantum mechanical average over the propagated quantum state. Following the definition, the OTOC at the initial moment of time is zero $C(0) = 0$, provided that $[\hat{W}(0), \hat{V}(0)] = 0$. In particular, for the local unitary and Hermitian operators of our choice $\hat{W}_m^{\dagger}(t) \equiv \hat{\sigma}_m^z(t) = \exp(i\hat{H}t)\hat{\eta}_m\exp(-i\hat{H}t)$, and $\hat{V}_n^{\dagger} = \hat{\sigma}_n^z = \hat{\eta}_n$, where $\hat{\eta}_n = \hat{2}a_n^{\dagger}\hat{a}_n - 1$. The bosonic operators are related to the spin operators via $\sigma_n^- = 2a_n^{\dagger}$, $\sigma_n^+ = 2a_n$, $\sigma_n^z = 2a_n^{\dagger}a_n - 1$. In terms of the occupation number operators, the OTOC is given as

$$\begin{aligned} C(t) = \frac{1}{2}\Big\{ &\langle \eta_n\eta_m(t)\eta_m(t)\eta_n\rangle + \langle \eta_m(t)\eta_n\eta_n\eta_m(t)\rangle \\ &- \langle \eta_m(t)\eta_n\eta_m(t)\eta_n\rangle - \langle \eta_n\eta_m(t)\eta_n\eta_m(t)\rangle\Big\}. \end{aligned} \tag{6}$$

Indeed, the OTOC can be interpreted as the overlap of two wave functions, which are time evolved in two different ways for the same initial state $|\psi(0)\rangle$. The first wave function is obtained by perturbing the initial state at $t = 0$ with a local unitary operator $\hat{V}$, then evolved further under the unitary evolution operator $\hat{U} = \exp(-\mathrm{i}\hat{H}t)$ until time t. It is then perturbed at time t with a local unitary operator $\hat{W}$, and evolved backwards from t to $t = 0$ under $\hat{U}^{\dagger}$. Hence, the time evolved wave function is $|\psi(t)\rangle = \hat{U}^{\dagger}\hat{W}\hat{U}\hat{V}|\psi(0)\rangle = \hat{W}(t)\hat{V}|\psi(0)\rangle$. To get the second wave function, the order of the applied perturbations is permuted, i.e. first $\hat{W}$ at t and then $\hat{V}$ at $t = 0$. Therefore, the second wave function is $|\phi(t)\rangle = \hat{V}\hat{U}^{\dagger}\hat{W}\hat{U}|\psi(0)\rangle = \hat{V}\hat{W}(t)|\psi(0)\rangle$ and their overlap is equivalent to $F(t) = \langle\phi(t)|\psi(t)\rangle$. The OTOC is calculated from this overlap using $C(t) = 1 - \Re[F(t)]$. What breaks the time inversion symmetry for the OTOC is the permuted sequence of operators $\hat{W}$ and $\hat{V}$. However, in spin-lattice models with a preserved spatial inversion symmetry $\hat{\mathcal{P}}\hat{H} = \hat{H}$, the spatial inversion $\hat{\mathcal{P}}d(\hat{W}, \hat{V}) = -d(\hat{W}, \hat{V}) = d(\hat{V}, \hat{W})$ can restore the permuted order between $\hat{V}$ and $\hat{W}$, where $d(\hat{W}, \hat{V})$ denotes the distance between observables $\hat{W}$ and $\hat{V}$. Permuting just a single wave function, one finds $C(t) = 1 - \Re(\langle\phi(t)|\hat{\mathcal{P}}\hat{\mathcal{T}}|\psi(t)\rangle) = C(0)$. Thus, a scrambled quantum entanglement formally can be unscrambled by a spatial inversion. However, in chiral systems $\hat{\mathcal{P}}\hat{H} \neq \hat{H}$ and the unscrambling procedure fails.

Taking into account equation (4), we analyze quantum information scrambling along the **x** axis *i.e.*, $\omega(\pm D, \mathbf{k}) = \omega(\pm D, k_x, 0)$ and along the **y** axis, $\omega(0, \mathbf{k}) = \omega(0, 0, k_y)$. It is easy to see that the quantum information flow along the **y** axis is symmetric, while along the **x** axis it is asymmetric and depends on the sign of the DM constant, i.e. the flow along the **x** is different from $-\mathbf{x}$. Let us assume that equation (1) holds for right-moving magnons and is violated for left-moving magnons. Excited magnons with the same frequency and propagating into different directions have different wave vectors $\omega_s(D, k_s^+) = \omega_s(-D, k_s^-)$ where:

$$\omega_s\left(\pm D, k_s^{\pm}\right) = 2J_1(1 - 1/2\cos k_x^{\pm}a) + 2J_2(1 - \cos k_x^{\pm}a) \pm D\sin k_x^{\pm}a, \tag{7}$$

$k_{m_0x}^+ = \frac{m_0\pi}{a_0}$, $m_0 = \mathbb{N}$ and $k_{m_0x}^-$ we find from the condition $\omega_s(D, k_s^+) = \omega_s(-D, k_s^-)$ leading to $k_{m_0x}^- = k_{m_0x}^+ + \frac{2}{a}\tan^{-1}(\frac{D}{J_1+2J_2})$. Here we use shortened notations $\omega_{m_0} = \omega_s(D, k_s^+) = \omega_s(-D, k_s^-)$ and set dimensionless units $J_1 = 2J_2 \equiv J = 1$. We excite in the diode magnons of different frequencies $m_0 = [1, N]$. Considering equations (6) and (7), following [39], we obtain expressions for the left and right OTOCs $C_L(t)$ and $C_R(t)$ as:

$$\begin{aligned} C_L(t) &= \frac{8}{N^2}\Omega_1^L\Omega_2^L - \frac{8}{N^4}\Omega_1^L\Omega_2^L\Omega_1^L\Omega_2^L, \\ C_R(t) &= \zeta^4(D)\left(\frac{8}{N^2}\Omega_1^R\Omega_2^R - \frac{8}{N^4}\Omega_1^R\Omega_2^R\Omega_1^R\Omega_2^R\right), \end{aligned} \tag{8}$$

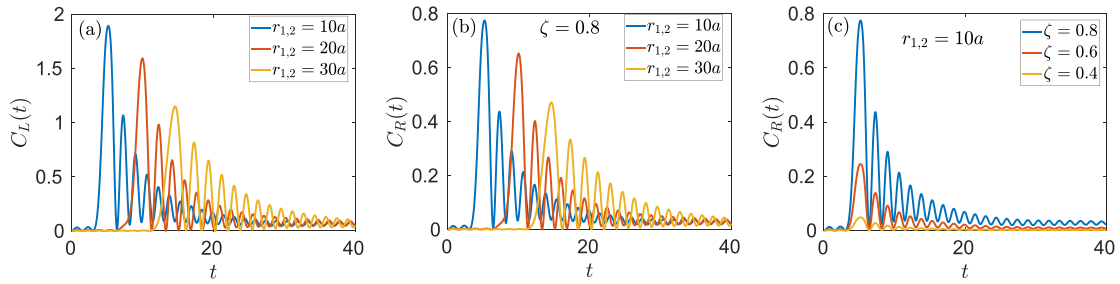

Figure 2. (a) Left-OTOC and (b) right-OTOC with time t (in the units of $1/J$) for different distances $r_{1,2} = 10a$, $20a$ and $30a$. (c) Right-OTOC with time for $r_{1,2} = 10a$ and suppression rates of the magnon current $\zeta = 0.8$, 0.6 and 0.4. Parameters are: $N = 1000$, $D = J_1 = 2J_2 = 1$. Periodic boundary conditions are considered. The values of the parameters: $m_0 = 1$ to N, $a = 10^{-3}$ and $a_0 = 1$.

where frequencies $\Omega_{1/2}^{L/R}$ and details of derivations are presented in appendix B. Parameter ξ enters into the right OTOC $C_R(t)$ expression because the right propagating magnons are scattered on the gate magnons. This is due to the non-reciprocal magnon dispersion relations associated with the DMI term. Since the value of ξ depends on the experimental setup, we consider experimentally feasible values in our calculations.

It should be noted that in the calculation of OTOC, we consider expectation value over the one magnon excitation state $\hat{a}_n^\dagger|\phi\rangle$, where $|\phi\rangle$ is the vacuum state. Such a state shows the presence of the quantum blockade effect in a magnonic crystal. The calculation of equal time second-order correlation function showing the quantum blockade effect is given in appendix C.

Figures 2(a) and (b) are the variation of $C_L(t)$ and $C_R(t)$ for $|n^+ - m|$ and $|n^- - m|$ distant spins, respectively. Both show similar behavior with increasing separation between the spins. However, the amplitude of $C_R(t)$ is less than $C_L(t)$ because the decay amplitude of the $C_R(t)$ varies due to the suppression coefficient ζ. In the case of the dominant attenuation by the gate magnons, the OTOC decreases significantly. The difference in $C_L(t)$ and $C_R(t)$ originated due to the asymmetry arising from the DMI term. The time required to deviate the OTOC from zero increases as the separation between the spins increases. This observation indicates that quantum information flow has a finite 'butterfly velocity'. On the contrary, the amplitude of OTOC decreases as the separation between the spins increases because the initial amount of quantum information spreads among more spins. At the large time, OTOC again becomes zero because it spreads over the whole system. Figure 2(c) is the behavior of $C_R(t)$ with decreasing suppression coefficient ζ and fixed value of distance between the spins $r_{1,2}$. As suppression coefficient ζ decreases, amplitude of $C_R(t)$ decreases which is indicator of increasing of rectification. Detailed discussion of rectification is in next subsection.

A high density of magnons can invalidate the assumption of a pure state or spin-wave approximation that works only for a low density of magnons. However, the key point in our case is that one has to distinguish between two sorts of magnons, gate magnons and propagating nonreciprocal magnons. The density of the propagating magnons can be regulated in the experiment through a microwave antenna, and one can always ensure that their density is low enough. It is easy to regulate the density of the gate magnons, and an experimentally accessible method is discussed in [16]. In the magnonic systems, the Kerr nonlinearity may lead to interesting effects, for example, the magnon–magnon entanglement and frequency shift [68, 69]. On the other hand, we note that DMI term and strong magneto-electric coupling may be responsible for nonlinear coupling terms similar to the magnon Kerr effect. This effect is studied in [70].

2.4. Rectification

The efficiency of the QID is given by the rectification coefficient i.e. the ratio between the left and right propagating magnons that is calculated by left and right OTOC. DMI term and non-reciprocal magnon dispersion relations influence rectification coefficient in two ways. (a) Directly meaning that in the left and right OTOCs appear different left and right dispersion relations and (b) non-directly meaning that magnonic crystal due to the scattering on the gate magnons bans propagation of the drain magnons in one direction only (damping of the OTOC current). This non-reciprocal damping effect is experimentally observed in magnonic crystals [16]. The non-reciprocal damping enhances rectification effect and it was not studied in the context of quantum information and OTOC before.

Let us calculate the total amount of correlations transferred in opposite directions followed by the rectification coefficient, a function of the external electric field as $R = \frac{\int_0^\infty C_R(t)\mathrm{d}t}{\int_0^\infty C_L(t)\mathrm{d}t}$. We interpolate the suppression rate as a function of the DMI coefficient in the form $\zeta(D) \approx e^{-D/5}$. The coefficient $\zeta(D)$ mimics

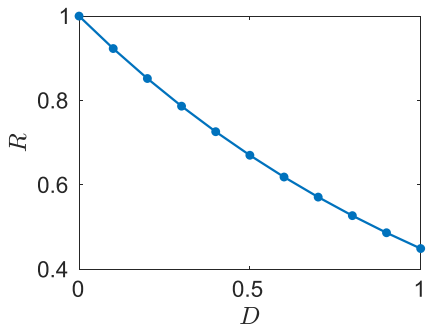

Figure 3. Rectification coefficient R is plotted against DMI coefficient (D) for suppression rate $\zeta(D) \approx e^{-D/5}$. The parameters are $J_1 = 2J_2 = 1$, $N = 1000$, $r_{12} = 10a$, $a_0 = 1$ and $m_0 = 1$ to N.

a scattering process of the drain magnons on the gate magnons [16]. In figure 3 we see the variation of the rectification coefficient as a function of D. The electric field has a direct and important role in rectification. In particular, DMI constant D depends on the electric field E_y as $D = E_y g_{\mathrm{ME}}$, where g_{ME} is the magneto-electric coupling constant. In the case of zero electric field, D will be zero, implying the absence of rectification effect $R = 1$. As the electric field increases, D also increases linearly, and rectification decreases exponentially. A detailed study of the role of the electric field in DM has been done in [36].

3. Discussions

We studied a quantum information flow in a spin quantum system. In particular, we proposed a quantum magnon diode based on YIG and magnonic crystal properties. The flow of magnons with wavelengths satisfying the Bragg conditions $k = m_0\pi/a_o$ is reflected from the gate magnons. Due to the absence of inversion symmetry in the system, left and right-propagating magnons have different dispersion relations and wave vectors. While for the right propagating magnons, the Bragg conditions hold, left magnons violate them, leading to an asymmetric flow of the quantum information. We found that the strength of quantum correlations depends on the distance between spins and time. The OTOC for the spins separated by longer distance shows an inevitable delay in time, meaning that the quantum information flow has a finite 'butterfly velocity'. On the other hand, the OTOC amplitude becomes smaller at longer distances between spins. The reason is that the initial amount of quantum information spreads among more spins. After the quantum information spreads over the whole system, which is pretty large ($N = 1000$ sites), the OTOC again becomes zero.

We proposed a novel theoretical concept that can be directly realized with the experimentally feasible setup and particular material. There are several experimentally feasible protocols for measuring OTOC in the spin systems [71, 72]. According to these protocols, one needs to initialize the system into the fully polarized state, then apply quench and measure the expectation value of the first spin. All these steps are directly applicable to our setup from YIG. The fully polarized initial state can be obtained by switching on and off a strong magnetic field at a time moment $t = 0$. Quench, in our case, is performed by a microwave antenna which is an experimentally accessible device. Polarization of the initial spin can be measured through the scanning tunneling microscope (STM) tip. Overall our setup is the experimentally feasible setup studied in [16].

Data availability statement

All data that support the findings of this study are included within the article (and any supplementary files). The data that support the findings of this study are available within the article.

Acknowledgments

SKM acknowledges the Science and Engineering Research Board, Department of Science and Technology, India for support under Core Research Grant CRG/2021/007095. A E acknowledges the funding by the Fonds zur Förderung der Wissenschaftlichen Forschung (FWF) under Grant No. I 5384.

Appendix A. Diagonalization of Hamiltonian equation (2)

2D square-lattice spin system with nearest-neighbor J_1 and the next nearest-neighbor J_2 coupling constants (taking $\hbar = 1$):

$$\begin{aligned}\hat{H} &= J_1 \sum_{\langle n,m\rangle} \hat{\sigma}_n\hat{\sigma}_m + J_2 \sum_{\langle\langle n,m\rangle\rangle} \hat{\sigma}_n\hat{\sigma}_m - \mathbf{P}\cdot\mathbf{E},\\ &= J_1 \sum_{\langle n,m\rangle} \hat{\sigma}_n\hat{\sigma}_m + J_2 \sum_{\langle\langle n,m\rangle\rangle} \hat{\sigma}_n\hat{\sigma}_m - D\sum_n (\hat{\sigma}_n \times \hat{\sigma}_{n+1})_z,\\ &= 4\Big[J_1 \sum_{\langle n,m\rangle} \hat{S}_n\hat{S}_m + J_2 \sum_{\langle\langle n,m\rangle\rangle} \hat{S}_n\hat{S}_m + \frac{D}{i}\sum_n (\hat{S}_n^+\hat{S}_{n+1}^- - \hat{S}_n^-\hat{S}_{n+1}^+)\Big],\\ &= 4\Big[J_1 \sum_{\langle n,m\rangle} \frac{1}{2}\Big\{\Big(\hat{S}_n^-\hat{S}_m^+ + \hat{S}_n^+\hat{S}_m^-\Big) + \hat{S}_n^z\hat{S}_m^z\Big\} + J_2 \sum_{\langle\langle n,m\rangle\rangle} \frac{1}{2}\Big\{\Big(\hat{S}_n^-\hat{S}_m^+ + \hat{S}_n^+\hat{S}_m^-\Big)\\ &\quad + \hat{S}_n^z\hat{S}_m^z\Big\} + \frac{D}{i}\sum_n (\hat{S}_n^+\hat{S}_{n+1}^- - \hat{S}_n^-\hat{S}_{n+1}^+)\Big]. \end{aligned} \tag{A.1}$$

Spin-half systems have two permitted states on each site, i.e. $|\uparrow\rangle$ and $|\downarrow\rangle$. Operation of spin operators on these state are given as

$$\hat{S}^+|\downarrow\rangle = |\uparrow\rangle,\ \ \hat{S}^+|\uparrow\rangle = 0, \tag{A.2}$$

$$\hat{S}^-|\uparrow\rangle = |\downarrow\rangle,\ \ \hat{S}^-|\downarrow\rangle = 0, \tag{A.3}$$

$$\hat{S}^z|\uparrow\rangle = \frac{1}{2}|\uparrow\rangle,\ \ \hat{S}^z|\downarrow\rangle = -\frac{1}{2}|\downarrow\rangle. \tag{A.4}$$

Transformation of the spin operators in hard-core bosonic creation and annihilation operators are given as

$$\begin{aligned}\hat{S}_{m,n}^+ &= \hat{a}_{m,n},\\ \hat{S}_{m,n}^- &= \hat{a}_{m,n}^\dagger,\\ \hat{S}_{m,n}^z &= 1/2 - \hat{a}_{m,n}^\dagger\hat{a}_{m,n}.\end{aligned} \tag{A.5}$$

Hamiltonian in the bosonic representation is given as

$$\begin{aligned}\hat{H} = 2\Big[&J_1 \sum_{\langle n,m\rangle} \Big(\hat{a}_n^\dagger\hat{a}_m + \hat{a}_n\hat{a}_m^\dagger - \hat{a}_n^\dagger\hat{a}_n - \hat{a}_m^\dagger\hat{a}_m + \frac{1}{2} + \hat{a}_n^\dagger\hat{a}_n\hat{a}_m^\dagger\hat{a}_m\Big)\\ &+ J_2 \sum_{\langle\langle n,m\rangle\rangle} \Big(\hat{a}_n^\dagger\hat{a}_m + \hat{a}_n\hat{a}_m^\dagger - \hat{a}_n^\dagger\hat{a}_n - \hat{a}_m^\dagger\hat{a}_m + \frac{1}{2} + \hat{a}_n^\dagger\hat{a}_n\hat{a}_m^\dagger\hat{a}_m\Big)\\ &+ \frac{D}{i}\sum_n \Big(\hat{a}_n\hat{a}_{n+1}^\dagger - \hat{a}_n^\dagger\hat{a}_{n+1}\Big)\Big].\end{aligned} \tag{A.6}$$

Fourier transform of $\hat{a}_n^\dagger(\hat{a}_n)$ is $\hat{a}_{\vec{k}}^\dagger(\hat{a}_{\vec{k}})$.

$$\begin{aligned}\hat{a}_{\vec{k}}^\dagger &= \frac{1}{\sqrt{N}}\sum_n e^{i\vec{k}\vec{r}_n}a_n^\dagger,\\ \hat{a}_{\vec{k}} &= \frac{1}{\sqrt{N}}\sum_n e^{-i\vec{k}\vec{r}_n}a_n.\end{aligned} \tag{A.7}$$

Inverse Fourier transform is given as

$$\begin{aligned}\hat{a}_n^\dagger &= \frac{1}{\sqrt{N}}\sum_n e^{i\vec{k}\vec{r}_n}a_{\vec{k}}^\dagger,\\ \hat{a}_n &= \frac{1}{\sqrt{N}}\sum_n e^{-i\vec{k}\vec{r}_n}a_{\vec{k}}.\end{aligned} \tag{A.8}$$

After summing over n we get Hamiltonian (equation (A.1)) in $\vec{k}$ space as

$$\begin{aligned}\hat{H} &= \sum_{\vec{k}} \omega_{\vec{k}} \hat{a}^{\dagger}_{\vec{k}} \hat{a}_{\vec{k}} - D \sum_{\vec{k}} \sin(\vec{k}a) \hat{a}^{\dagger}_{\vec{k}} \hat{a}_{\vec{k}}, \\ &= \sum_{\vec{k}} \omega(\pm D, \mathbf{k}) \hat{a}^{\dagger}_{\vec{k}} \hat{a}_{\vec{k}} \end{aligned} \tag{A.9}$$

where,

$$\begin{aligned}&\omega(\pm D, \mathbf{k}) = \left(\omega(\vec{k}) \pm \omega_{\mathrm{DM}}(\vec{k})\right), \ \ \omega_{\mathrm{DM}}(\vec{k}) = D \sin(k_x a), \\ &\omega(\vec{k}) = 2J_1(1-\gamma_{1,\mathbf{k}}) + 2J_2(1-\gamma_{2,\mathbf{k}}), \ \gamma_{1,\mathbf{k}} = \frac{1}{2}(\cos k_x a + \cos k_y a), \\ &\gamma_{2,\mathbf{k}} = \frac{1}{2}[\cos(k_x + k_y)a + \cos(k_x - k_y)a]. \end{aligned} \tag{A.10}$$

Appendix B. Calculation of left and right out-of-time ordered correlation functions

We will calculate OTOC exactly for one magnon excitation states given in equation (7) as

$$\begin{aligned}C(t) = \frac{1}{2}\Big\{ &\langle \hat{\eta}_n \hat{\eta}_m(t) \hat{\eta}_m(t) \hat{\eta}_n \rangle + \langle \hat{\eta}_m(t) \hat{\eta}_n \hat{\eta}_n \hat{\eta}_m(t) \rangle \\ &- \langle \hat{\eta}_m(t) \hat{\eta}_n \hat{\eta}_m(t) \hat{\eta}_n \rangle - \langle \hat{\eta}_n \hat{\eta}_m(t) \hat{\eta}_n \hat{\eta}_m(t) \Big\}. \end{aligned} \tag{B.1}$$

Here, $\hat{\eta}_{m/n} = \hat{\sigma}^z_{m/n}$ is Hermitian and unitary, therefore, equation (B.1) transforms in the form given as

$$C(t) = 1 - \langle \hat{\eta}_m(t) \hat{\eta}_n \hat{\eta}_m(t) \hat{\eta}_n \rangle = 1 - F(t),$$

where $F(t)$ is given as

$$F(t) = \langle \phi | \hat{a}_n \hat{\eta}_m(t) \hat{\eta}_n \hat{\eta}_m(t) \hat{\eta}_n a^{\dagger}_n | \phi \rangle. \tag{B.3}$$

In the above equation, expectation value is taken over one magnon excitation state $\hat{a}^{\dagger}_n|\phi\rangle$, where $|\phi\rangle$ is the vacuum state, equivalent to a polarized state. First of all we calculate the product of four observables in $F(t)$ (equation (B.3)) in bosonic representation as

$$\begin{aligned}\hat{\eta}_m(t)\hat{\eta}_n\hat{\eta}_m(t)\hat{\eta}_n &= [1 - 2\hat{a}^{\dagger}_m \hat{a}_m(t)][1 - 2\hat{a}^{\dagger}_n \hat{a}_n][1 - 2\hat{a}^{\dagger}_m \hat{a}_m(t)][1 - 2\hat{a}^{\dagger}_n \hat{a}_n], \\ &= \left[1 - 2\hat{a}^{\dagger}_m \hat{a}_m(t) - 2\hat{a}^{\dagger}_n \hat{a}_n + 4\hat{a}^{\dagger}_m \hat{a}_m(t) \hat{a}^{\dagger}_n \hat{a}_n\right] \\ &\quad \times \left[1 - 2\hat{a}^{\dagger}_m \hat{a}_m(t) - 2\hat{a}^{\dagger}_n \hat{a}_n + 4\hat{a}^{\dagger}_m \hat{a}_m(t) \hat{a}^{\dagger}_n \hat{a}_n\right], \\ &= 1 - 4\hat{a}^{\dagger}_m \hat{a}_m(t) - 4\hat{a}^{\dagger}_n \hat{a}_n + 4\hat{a}^{\dagger}_m \hat{a}_m(t) \hat{a}^{\dagger}_n \hat{a}_n + 4\hat{a}^{\dagger}_n \hat{a}_n \hat{a}^{\dagger}_m \hat{a}_m(t) \\ &\quad + 4\hat{a}^{\dagger}_m \hat{a}_m \hat{a}^{\dagger}_m \hat{a}_m(t) + 4\hat{a}^{\dagger}_n \hat{a}_n \hat{a}^{\dagger}_n \hat{a}_n + 4\hat{a}^{\dagger}_m \hat{a}_m \hat{a}^{\dagger}_n \hat{a}_n + 4\hat{a}^{\dagger}_n \hat{a}_n \hat{a}^{\dagger}_m \hat{a}_m \\ &\quad - 8\hat{a}^{\dagger}_m \hat{a}_m \hat{a}^{\dagger}_m \hat{a}_m(t) \hat{a}^{\dagger}_n \hat{a}_n - 8\hat{a}^{\dagger}_n \hat{a}_n \hat{a}^{\dagger}_m \hat{a}_m(t) \hat{a}^{\dagger}_n \hat{a}_n \\ &\quad - 8\hat{a}^{\dagger}_m \hat{a}_m(t) \hat{a}^{\dagger}_n \hat{a}_n \hat{a}^{\dagger}_m \hat{a}_m(t) - 8\hat{a}^{\dagger}_m \hat{a}_m(t) \hat{a}^{\dagger}_n \hat{a}_n \hat{a}^{\dagger}_n \hat{a}_n \\ &\quad + 16\hat{a}^{\dagger}_m \hat{a}_m(t) \hat{a}^{\dagger}_n \hat{a}_n \hat{a}^{\dagger}_m \hat{a}_m(t) \hat{a}^{\dagger}_n \hat{a}_n. \end{aligned} \tag{B.4}$$

Further, we calculate the expectation value of the last term of equation (B.4) over one magnon excitation state *i.e.*, $\langle \phi | \hat{a}_n \hat{a}^{\dagger}_m \hat{a}_m(t) \hat{a}^{\dagger}_n \hat{a}_n \hat{a}^{\dagger}_n \hat{a}^{\dagger}_m \hat{a}_m(t) \hat{a}^{\dagger}_n \hat{a}_n \hat{a}^{\dagger}_n | \phi \rangle$, using the properties of bosonic operators $[\hat{a}_i, \hat{a}^{\dagger}_j] = \delta_{ij}$, $(\hat{a}_i)^2 = 0$, and $(\hat{a}^{\dagger}_i)^2 = 0$. We get

$$\begin{aligned}\langle \phi | \hat{a}_n \hat{a}^{\dagger}_m \hat{a}_m(t) \hat{a}^{\dagger}_n \hat{a}_n \hat{a}^{\dagger}_n \hat{a}^{\dagger}_m \hat{a}_m(t) \hat{a}^{\dagger}_n \hat{a}_n \hat{a}^{\dagger}_n | \phi \rangle &= \langle \phi | \hat{a}_n e^{i\hat{H}t} \hat{a}^{\dagger}_m \hat{a}_m e^{-i\hat{H}t} \hat{a}^{\dagger}_n \hat{a}_n e^{i\hat{H}t} \hat{a}^{\dagger}_m \hat{a}_m e^{-i\hat{H}t} \hat{a}^{\dagger}_n | \phi \rangle, \\ &= \langle \Psi(t) | \Psi(t) \rangle, \end{aligned} \tag{B.5}$$

where $|\Psi(t)\rangle = \hat{a}_n e^{i\hat{H}t}\hat{a}_m^\dagger \hat{a}_m e^{-i\hat{H}t}\hat{a}_n^\dagger|\phi\rangle$. Fourier transformation of the $|\Psi(t)\rangle$ and diagonalized Hamiltonian will provide

$$\begin{aligned}|\Psi(t)\rangle &= \frac{1}{N}\sum_k e^{i(-k(m-n)+\omega_k t/\hbar)}\frac{1}{N}\sum_{k'} e^{i(k'(m-n)-\omega_{k'}t/\hbar)}|\phi\rangle \\ &= \frac{1}{N^2}\Omega_1\Omega_2|\phi\rangle.\end{aligned}$$

Hence,

$$\langle\Psi(t)|\Psi(t)\rangle = \frac{1}{N^4}\Omega_1\Omega_2\Omega_1\Omega_2. \tag{B.6}$$

Similarly,

$$\langle\phi|\hat{a}_n\hat{a}_m\hat{a}_m(t)\hat{a}_n^\dagger|\phi\rangle = \frac{1}{N^2}\Omega_1\Omega_2. \tag{B.7}$$

After doing simple bosonic algebra, time-dependent terms of equation (B.4) are converted either in the form of equation (B.5) or (B.7). By using equations (B.6) and (B.7), we calculate $F(t)$ as

$$\begin{aligned}F(t) = 1 &- \frac{4}{N^2}\Omega_1\Omega_2 - 4 + \frac{4}{N^2}\Omega_1\Omega_2 + \frac{4}{N^2}\Omega_1\Omega_2 + \frac{4}{N^2}\Omega_1\Omega_2 + \frac{4}{N^2}\Omega_1\Omega_2 + \frac{4}{N^2}\Omega_1\Omega_2 + 4 \\ &- \frac{8}{N^2}\Omega_1\Omega_2 - \frac{8}{N^2}\Omega_1\Omega_2 - \frac{8}{N^4}\Omega_1\Omega_2\Omega_1\Omega_2 - \frac{8}{N^2}\Omega_1\Omega_2 + \frac{16}{N^4}\Omega_1\Omega_2\Omega_1\Omega_2 \\ = 1 &- \frac{8}{N^2}\Omega_1\Omega_2 + \frac{8}{N^4}\Omega_1\Omega_2\Omega_1\Omega_2.\end{aligned}$$

Then, we get the left and right OTOCs' analytical expressions as

$$\begin{aligned}C_L(t) &= \frac{8}{N^2}\Omega_1^L\Omega_2^L - \frac{8}{N^4}\Omega_1^L\Omega_2^L\Omega_1^L\Omega_2^L, \\ C_R(t) &= \zeta^4(D)\left(\frac{8}{N^2}\Omega_1^R\Omega_2^R - \frac{8}{N^4}\Omega_1^R\Omega_2^R\Omega_1^R\Omega_2^R\right),\end{aligned} \tag{B.9}$$

where frequencies $\Omega_{1/2}^{L/R}$ are given as

$$\Omega_1^R = \Omega_2^{R*} = \sum_{m_0}\exp\left(-\frac{im_0\pi r_{1,2}}{a_0}\right)\exp\left(\frac{i\omega_{m_0}t}{\hbar}\right),$$

and

$$\Omega_1^L = \Omega_2^{L*} = \sum_{m_0}\exp(-ik_s^- r_{1,2})\exp\left(\frac{i\omega_{m_0}t}{\hbar}\right). \tag{B.10}$$

Appendix C. Quantum blockade effects

To analyze the magnon blockade effect, we calculate the equal time second-order correlation function defined as [73–78]

$$g_a^2(0) = \frac{\mathrm{Tr}(\hat{\rho}\hat{a}_m^{\dagger 2}\hat{a}_m^2)}{\left[\mathrm{Tr}(\hat{\rho}\hat{a}_m^\dagger\hat{a}_m)\right]^2} = \frac{\langle\hat{a}_m^{\dagger 2}\hat{a}_m^2\rangle}{\langle a_m^\dagger\hat{a}_m\rangle^2}, \tag{C.1}$$

where $a_m(a_m^\dagger)$ are the annihilation (creation) operators of the magnon excitation. The magnon blockade is inferred from the condition $g_a^2(0) \to 0$ meaning that magnons can be excited individually, and two or more magnons cannot be excited together.

We note that $\hat{a}_m^2\hat{a}_m^\dagger|\phi\rangle = 0$ leading to $g_a^2(0) = 0$. Therefore, the quantum blockade effect occurs in this case.

ORCID iDs

Levan Chotorlishvili https://orcid.org/0000-0001-7042-9273
Arthur Ernst https://orcid.org/0000-0003-4005-6781
Sunil K Mishra https://orcid.org/0000-0002-3409-7352

References

[1] Liang B, Yuan B and Cheng J C 2009 *Phys. Rev. Lett.* **103** 104301
[2] Liang B, Guo X, Tu J, Zhang D and Cheng J 2010 *Nat. Mater.* **9** 989–92
[3] Li X F, Ni X, Feng L, Lu M H, He C and Chen Y F 2011 *Phys. Rev. Lett.* **106** 084301
[4] Maldovan M 2013 *Nature* **503** 209–17
[5] Ren J 2013 *Phys. Rev.* B **88** 220406
[6] Lepri S, Livi R and Politi A 1997 *Phys. Rev. Lett.* **78** 1896–9
[7] Komatsu T S and Ito N 2011 *Phys. Rev.* E **83** 012104
[8] Kim P, Shi L, Majumdar A and McEuen P L 2001 *Phys. Rev. Lett.* **87** 215502
[9] Kobayashi W, Teraoka Y and Terasaki I 2009 *Appl. Phys. Lett.* **95** 171905
[10] Li B, Lan J and Wang L 2005 *Phys. Rev. Lett.* **95** 104302
[11] Terraneo M, Peyrard M and Casati G 2002 *Phys. Rev. Lett.* **88** 094302
[12] Li B, Wang L and Casati G 2004 *Phys. Rev. Lett.* **93** 184301
[13] Li N, Ren J, Wang L, Zhang G, Hänggi P and Li B 2012 *Rev. Mod. Phys.* **84** 1045–66
[14] Chotorlishvili L, Etesami S, Berakdar J, Khomeriki R and Ren J 2015 *Phys. Rev.* B **92** 134424
[15] Chumak A, Serga A, Hillebrands B and Kostylev M 2008 *Appl. Phys. Lett.* **93** 022508
[16] Chumak A V, Serga A A and Hillebrands B 2014 *Nat. Commun.* **5** 1–8
[17] Nikitov S, Tailhades P and Tsai C 2001 *J. Magn. Magn. Mater.* **236** 320–30
[18] Kruglyak V and Kuchko A 2004 *J. Magn. Magn. Mater.* **272** 302–3
[19] Wang Z, Zhang V, Lim H, Ng S, Kuok M, Jain S and Adeyeye A 2009 *Appl. Phys. Lett.* **94** 083112
[20] Gubbiotti G, Tacchi S, Madami M, Carlotti G, Adeyeye A and Kostylev M 2010 *J. Phys. D: Appl. Phys.* **43** 264003
[21] Ustinov A B, Drozdovskii A V and Kalinikos B A 2010 *Appl. Phys. Lett.* **96** 142513
[22] Gurevich A G and Melkov G A 1996 *Magnetization Oscillations and Waves* (CRC press)
[23] Takashima R, Shiomi Y and Motome Y 2018 *Phys. Rev.* B **98** 020401
[24] Matsumoto T and Hayami S 2020 *Phys. Rev.* B **101** 224419
[25] Shiomi Y, Takashima R, Okuyama D, Gitgeatpong G, Piyawongwatthana P, Matan K, Sato T and Saitoh E 2017 *Phys. Rev.* B **96** 180414
[26] Wang X G, Chotorlishvili L, Guo G H and Berakdar J 2018 *J. Appl. Phys.* **124** 073903
[27] Katsura H, Nagaosa N and Balatsky A V 2005 *Phys. Rev. Lett.* **95** 057205
[28] Mostovoy M 2006 *Phys. Rev. Lett.* **96** 067601
[29] Ramesh R and Spaldin N A 2010 *Nanoscience and Technology: A Collection of Reviews from Nature Journals* (Nature Pub. Group) pp 20–28
[30] Bibes M and Barthélémy A 2008 *Nat. Mater.* **7** 425–6
[31] Fiebig M 2005 *J. Phys. D: Appl. Phys.* **38** R123
[32] Hemberger J, Schrettle F, Pimenov A, Lunkenheimer P, Ivanov V Y, Mukhin A, Balbashov A and Loidl A 2007 *Phys. Rev.* B **75** 035118
[33] Meyerheim H, Klimenta F, Ernst A, Mohseni K, Ostanin S, Fechner M, Parihar S, Maznichenko I, Mertig I and Kirschner J 2011 *Phys. Rev. Lett.* **106** 087203
[34] Cheong S-W and Mostovoy M 2007 *Nat. Mater.* **6** 13–20
[35] Menzel M, Mokrousov Y, Wieser R, Bickel J E, Vedmedenko E, Blügel S, Heinze S, von Bergmann K, Kubetzka A and Wiesendanger R 2012 *Phys. Rev. Lett.* **108** 197204
[36] Liu T and Vignale G 2011 *Phys. Rev. Lett.* **106** 247203
[37] Maruyama K, Iitaka T and Nori F 2007 *Phys. Rev.* A **75** 012325
[38] Udvardi L and Szunyogh L 2009 *Phys. Rev. Lett.* **102** 207204
[39] Guo Z X, Hu X D, Su Q Q and Li Z 2021 arXiv:2109.11371
[40] Guo Z X, Hu X D, Su Q Q and Li Z 2017 *Phys. Rev.* B **96** 054440
[41] Kuwahara T and Saito K 2021 *Phys. Rev. Lett.* **127** 070403
[42] Hastings M B and Koma T 2006 *Commun. Math. Phys.* **265** 781
[43] Nachtergaele B, Ogata Y and Sims R 2006 *J. Stat. Phys.* **124** 1
[44] Lieb E H and Robinson D W 1972 The finite group velocity of quantum spin systems *Statistical Mechanics* (Springer) pp 425–31
[45] Zakeri K, Zhang Y, Prokop J, Chuang T H, Sakr N, Tang W X and Kirschner J 2010 *Phys. Rev. Lett.* **104** 137203
[46] Iguchi Y, Uemura S, Ueno K and Onose Y 2015 *Phys. Rev.* B **92** 184419
[47] Seki S *et al* 2016 *Phys. Rev.* B **93** 235131
[48] Sato T J, Okuyama D, Hong T, Kikkawa A, Taguchi Y, Arima T H and Tokura Y 2016 *Phys. Rev.* B **94** 144420
[49] Gitgeatpong G, Zhao Y, Piyawongwatthana P, Qiu Y, Harriger L W, Butch N P, Sato T J and Matan K 2017 *Phys. Rev. Lett.* **119** 047201
[50] Larkin A I and Ovchinnikov Y N 1969 *Sov. Phys. JETP* **28** 1200
[51] Maldacena J, Shenker S H and Stanford D 2016 *J. High Energy Phys.* JHEP08(2016)106
[52] Roberts D A, Stanford D and Susskind L 2015 *J. High Energy Phys.* JHEP03(2015)051
[53] Iyoda E and Sagawa T 2018 *Phys. Rev.* A **97** 042330
[54] Chapman A and Miyake A 2018 *Phys. Rev.* A **98** 012309
[55] Swingle B and Chowdhury D 2017 *Phys. Rev.* B **95** 060201
[56] Klug M J, Scheurer M S and Schmalian J 2018 *Phys. Rev.* B **98** 045102
[57] del Campo A, Molina-Vilaplana J and Sonner J 2017 *Phys. Rev.* D **95** 126008
[58] Campisi M and Goold J 2017 *Phys. Rev.* E **95** 062127
[59] Hosur P, Qi X L, Roberts D A and Yoshida B 2016 *J. High Energy Phys.* JHEP02(2016)004

[60] Yunger Halpern N 2017 *Phys. Rev.* A **95** 012120
[61] Heyl M, Pollmann F and Dóra B 2018 *Phys. Rev. Lett.* **121** 016801
[62] Chen B, Hou X, Zhou F, Qian P, Shen H and Xu N 2020 *Appl. Phys. Lett.* **116** 194002
[63] Shukla R K, Naik G K and Mishra S K 2021 *Europhys. Lett.* **132** 47003
[64] Rozenbaum E B, Ganeshan S and Galitski V 2017 *Phys. Rev. Lett.* **118** 086801
[65] Shukla R K, Lakshminarayan A and Mishra S K 2022 *Phys. Rev.* B **105** 224307
[66] Shukla R K and Mishra S K 2022 *Phys. Rev.* A **106** 022403
[67] Kukuljan I, Grozdanov S and Prosen T 2017 *Phys. Rev.* B **96** 060301
[68] Zhang Z, Scully M O and Agarwal G S 2019 *Phys. Rev. Res.* **1** 023021
[69] Moslehi M, Baghshahi H R, Faghihi M J and Mirafzali S Y 2022 *Eur. Phys. J. Plus* **137** 1–7
[70] Toklikishvili Z, Chotorlishvili L, Khomeriki R, Jandieri V and Berakdar J 2023 *Phys. Rev.* B **107** 115126
[71] Nie X *et al* 2020 *Phys. Rev. Lett.* **124** 250601
[72] Li J, Fan R, Wang H, Ye B, Zeng B, Zhai H, Peng X and Du J 2017 *Phys. Rev.* X **7** 031011
[73] Liu Z X, Xiong H and Wu Y 2019 *Phys. Rev.* B **100** 134421
[74] Xie J K, Ma S L and Li F L 2020 *Phys. Rev.* A **101** 042331
[75] Wu K, Zhong W X, Cheng G L and Chen A X 2021 *Phys. Rev.* A **103** 052411
[76] Zhao C, Li X, Chao S, Peng R, Li C and Zhou L 2020 *Phys. Rev.* A **101** 063838
[77] Wang F, Gou C, Xu J and Gong C 2022 *Phys. Rev.* A **106** 013705
[78] Wang L, Yang Z X, Liu Y M, Bai C H, Wang D Y, Zhang S and Wang H F 2020 *Ann. Phys., Lpz.* **532** 2000028